Body Wave Traveltimes and A Spherically Symmetric P- and S-Wave Velocity Model

Article *in* Geophysical Journal International · February 1993

DOI: 10.1111/j.1365-246X.1993.tb01448.x

2 authors:

Andrea Morelli
National Institute of Geophysics and Volca…
142 PUBLICATIONS **4,009** CITATIONS
SEE PROFILE

Adam Dziewonski
Harvard University
249 PUBLICATIONS **26,163** CITATIONS
SEE PROFILE

Geophys. J. Int. (1993) **112,** 178–194

Body wave traveltimes and a spherically symmetric *P*- and *S*-wave velocity model

[1]Andrea Morelli and [2]Adam M. Dziewonski

[1]*Istituto Nazionale di Geofisica, Via di Vigna Murata* 605, 00143 *Roma, Italy*
[2]*Department of Earth and Planetary Sciences, Harvard University, Cambridge, MA* 02138, *USA*

Accepted 1992 July 10. Received 1992 July 10; in original form 1991 August 5

SUMMARY

The derivation of a spherically-symmetric reference earth model is a subject which has recently regained interest. After a decade of studies on lateral heterogeneity we now have the tools to approach the problem. An IASPEI Working Group on Traveltime Tables was formed in 1988 with the goal of deriving a reliable and up-to-date radial model of seismic velocities. Following the guidelines developed by that working group we have investigated the body wave traveltimes for several branches frequently reported in the ISC Bulletins and propose here a model for *P*-and *S*-wave velocities consistent with these data.

Approximately 16 000 best-recorded, shallow-focus earthquakes are selected from 24 years of ISC Bulletins (1964–1987) and relocated using, among others, corrections for lateral heterogeneity. From this dataset we derive summary traveltime curves specified for each degree of epicentral distance for *P*, *PcP–P*, PKP_{AB}, PKP_{BC}, *PKIKP* and *S*. To constrain velocity at the top of the outer core, we include data for *SKS* and *SKKS–SKS* from Hales & Roberts (1970, 1971). Our discrete time–distance curves are obtained by evaluating the shape of the residual density distribution, independently for each 1° interval, to limit contamination due to the interference of other branches, precursors or late readings.

In the upper mantle, the resulting model, SP6, differs from *iasp91* (Kennett & Engdahl 1991) only by slightly higher *P* and *S* velocities between 410 and 660 km. In the lower mantle, new velocity profiles have lower velocity gradients. This is also true in comparison with PREM (Dziewonski & Anderson 1981). At the top of the outer core v_P is smaller than in PREM, and the velocity jump at the inner core boundary is reduced to the value of 0.62 km s^{-1}. The new inner core radius is 1215 km. Our model predicts traveltimes that differ from the *iasp91* tables considerably, although generally less than 1 s, except for *SKS* and *SKKS* for which the differences are greater.

Key words: body waves, earthquake location, earth's core, earth's upper and lower mantle, global earth models, lateral heterogeneity, traveltimes.

INTRODUCTION

During the last decade or so, important developments in seismology improved our knowledge of the structure of the interior of the earth. Radial and lateral heterogeneities have been mapped at all depths inside the earth, and efforts are currently under way to refine the detail of these images.

On the other hand, routine determination of earthquake hypocentres is done relying on reference traveltime tables (Jeffreys & Bullen 1940; J–B hereafter) which precede the discovery of many features in the deep-earth structure. In particular, upper mantle and core structure is now also known much better in its spherically symmetric component. It may appear, therefore, timely and necessary to try to define a new reference model, which will benefit from the knowledge reached by recent research on earth structure and which will at the same time be suitable for use in earthquake location.

A better reference traveltime model should result in more satisfactory earthquake locations. However, the J–B

traveltime tables, derived empirically without strict constraints on the physical implications of certain features, perform rather well half a century later. At teleseismic distances, the only major problem, widely recognized, is a constant time shift, due to the intrinsic trade off between the origin time and change in wave velocity: the origin times obtained using the J–B tables are systematically early by as much as 2 s. This problem may easily be overcome: the current availability of data from explosions and special events precisely located from high-quality local networks makes possible calibration of the new tables. Also, the availability of a voluminous dataset, such as that represented by the ISC Bulletins, would result in more accurate empirical tables. However, another empirical fit to the observed times—even if it would, by definition, closely reproduce the data—is not a satisfactory solution, for the following reasons.

A reference model, in a modern sense, is one which satisfies more than just one class of seismological or geophysical observations—like, for instance, traveltimes of body waves. It should constitute a common basis of reference for all the different studies concerning the earth. An example of this modelling philosophy is PREM (Dziewonski & Anderson 1981) which can in fact be used for much more than just earthquake location.

Its principal function is as a common benchmark and as a starting model for many other applications—some of which, incidentally, use standard locations as input—such as seismic tomography or synthetic seismogram calculations for the retrieval of the earthquake source mechanism. This strategy seeks a model which has to be physically meaningful—as opposed to an empirical one, which could achieve good results at reproducing a narrow range of observations, rather than at explaining them. The latter alternative results in a series of narrow-band models, each suited for a particular application. In that case, comparison and integration of diverse studies will become difficult and not self-consistent. It is therefore essential for a new reference model to be physically meaningful. That, for instance, means that it will have to be as close as possible to the spherical average of the earth, which in 3-D studies corresponds to the $\ell = 0$ term in a spherical harmonic expansion.

After one century of seismological observations it is clear that there is no unique way to derive the spherical average. Seismic events are clustered along narrow belts of activity, and radiated elastic energy samples the earth in a biased way. Also, concentration of seismic stations varies, resulting in highly populated and sparsely sampled zones. Because of this situation, a fit to all individual observations—for instance in the least-squares sense—may result in an average which is in fact strongly biased by the uneven geographical distribution of data. The 'correct' determination of a spherical earth model—meaning by this what we would obtain with a complete and uniform sampling of the globe—is in fact part of a larger problem, namely that of mapping the 3-D structure. The ideal and geographically correct average earth would be the $\ell = 0$ component of a laterally heterogeneous model. However, in order to simplify the discussion and concentrate more on the final goal, an alternate scheme of accounting for lateral heterogeneity may be employed. We choose the source region-station correction scheme and the global joint hypocentre determination as proposed by Dziewonski & Morelli (1989, DM89 hereafter).

The *P*- and *S*-wave velocity model presented here should not be understood as the end product of what we perceive to be the correct process of construction of a new reference earth model. It is rather a tool that we use to demonstrate the internal consistency, or its absence, of different subsets of our data. It should not be considered as an alternative to *iasp91* (Kennett & Engdahl 1991), but rather as the result of a different modelling concept. To this extent, direct comparison of the performance of the two models at locating earthquakes is beyond the goals of this article. We point out that a reference model should be more general and have more applications than just for earthquake location. For this, we feel that more observations, in particular from long period seismology, should be included. However, this is left as a further step, whereas now we choose to concentrate on traveltimes of body waves alone.

As we use in model SP6 the same parametrization as employed in *iasp91,* the two models can be readily compared. Indeed, to facilitate such a comparison, we have adopted the upper mantle of *iasp91,* even though the absence of the low velocity zone in the upper mantle could be found objectionable by many geophysicists. The fine structure of this region is not resolvable by the teleseismic traveltime data, but minute adjustments to upper mantle parameters of *iasp91* were necessary to bring it into agreement with our observations.

NEW TRAVELTIMES AND APPROACH TO INVERSION

The choice of the data and the parametrization we use follow the guidelines set by the Working Group on Traveltimes of the Subcommission on Seismological Algorithms (Kennett 1988). The input data for the current work are the arrival times published in the Bulletins of the International Seismological Center for the years from 1964 to 1987. Also, for phases that are more difficult to identify properly and whose arrival times are more difficult to read (*SKS* and *SKKS*), we use summary time–distance curves derived from the literature (Hales & Roberts 1970, 1971). The size and homogeneity of the ISC dataset is unique, particularly in that its internal consistency is guaranteed for the entire reporting period (Adams, Hughes & McGregor 1982). However, the reliability of phases other than first arrivals—and even for the first arrivals of core phases—is often doubtful. It is advisable then to proceed with caution to avoid biasing the model with systematically misidentified phases.

From the ISC Bulletins for the years 1964 to 1987 we selected only shallow events ($h < 50$ km) because they are geographically distributed in a more uniform way than deep seismicity. Also, because of the need to relocate hypocentres, we require that each event be recorded by at least 30 observatories at *P*-teleseismic distance, distributed so as to cover at least three of the four azimuthal quadrants. A relocation is performed using a starting model, described below, corrections for station elevation, and ellipticity (Dziewonski & Gilbert 1976). The relocation did not perturb focal depths, and considered only observations with

a residual smaller than 10 s, with residuals larger than 3 s weighted by a function decreasing exponentially from 1 to 0.01. The resulting dataset includes 16 574 events.

For derivation of correction terms for lateral heterogeneity, we propose a scheme (DM89) analogous to a global Joint Hypocentre Determination (JHD). The JHD is based upon empirical derivation of station corrections for a master event, and subsequent use of these corrections to locate other events in the vicinity of the master event. This has been shown to lead to much better relative locations and significant decrease in variance. We divide the earth's surface into 1656 roughly equal area elements, of dimension $5° \times 5°$ at the equator, and call these elements *source regions*. Then we relocate all the K earthquakes, with the procedure outlined above, within the ith source region, and derive a correction S for the jth station combining all the individual residuals δt:

$$S_{ij} = \left(\sum_{k}^{K} \delta t_{ijk}\right)/K. \quad (1)$$

Fig. 1 shows an example of empirical corrections for station ALQ (Albuquerque). It is of interest to observe the substantial spatial coherence of the source region residuals. For example, residuals from the source regions of the general area of the Mediterranean are consistently negative, while the sources in Alaska are slower than average by at least 1 s. Such corrections could be quite rough, if K is small. Also, discontinuities in relative locations could be introduced across the source region boundaries. To avoid this, we use a weighting scheme which combines the terms of a number of neighbouring regions with the form of a 2-D running average, with an exponential weight decreasing as the distance of the centre of each square from the epicentre. In this way, the correction for any station is a continuous function of position. Also, the artificial roughness of poorly determined source corrections is avoided.

The use of empirical corrections can lead to significant variance reduction. Fig. 2 compares histograms of average variance from the ISC Bulletins against the residual variance after the relocation which makes use of empirical corrections. While the maximum of the histogram corresponds to the value of 1.3 s^2 for the ISC locations, after applying empirical corrections it is reduced to 0.5 s^2. For the procedure to be fully consistent, however, similar corrections should be computed for core phases and, perhaps, for the S phase.

The conceptually simplest way to derive a model is to use

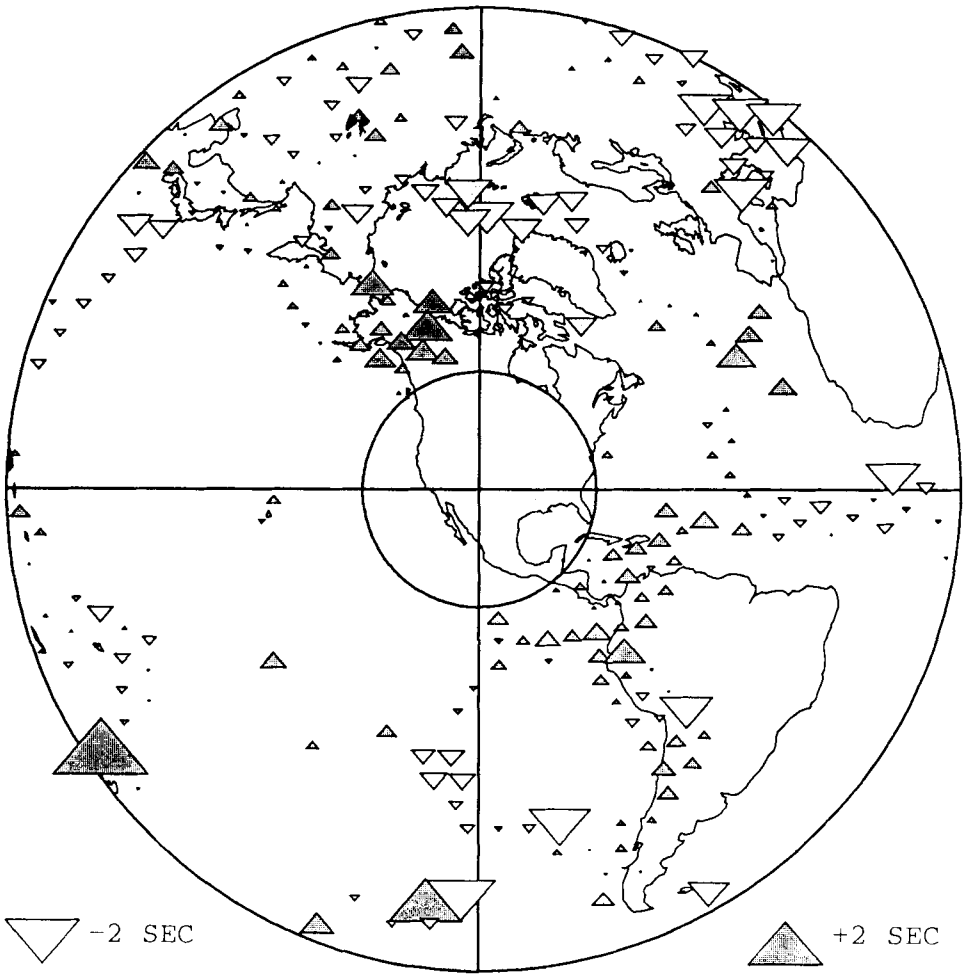

Figure 1. Empirical source-station corrections for station ALQ (Albuquerque). For this station, there are 259 source regions for which at least two measurements exist. Each source region average residual is plotted as a triangle. Arrivals slower than average are shown by upward-pointing triangles, faster than average by downward pointing triangles.

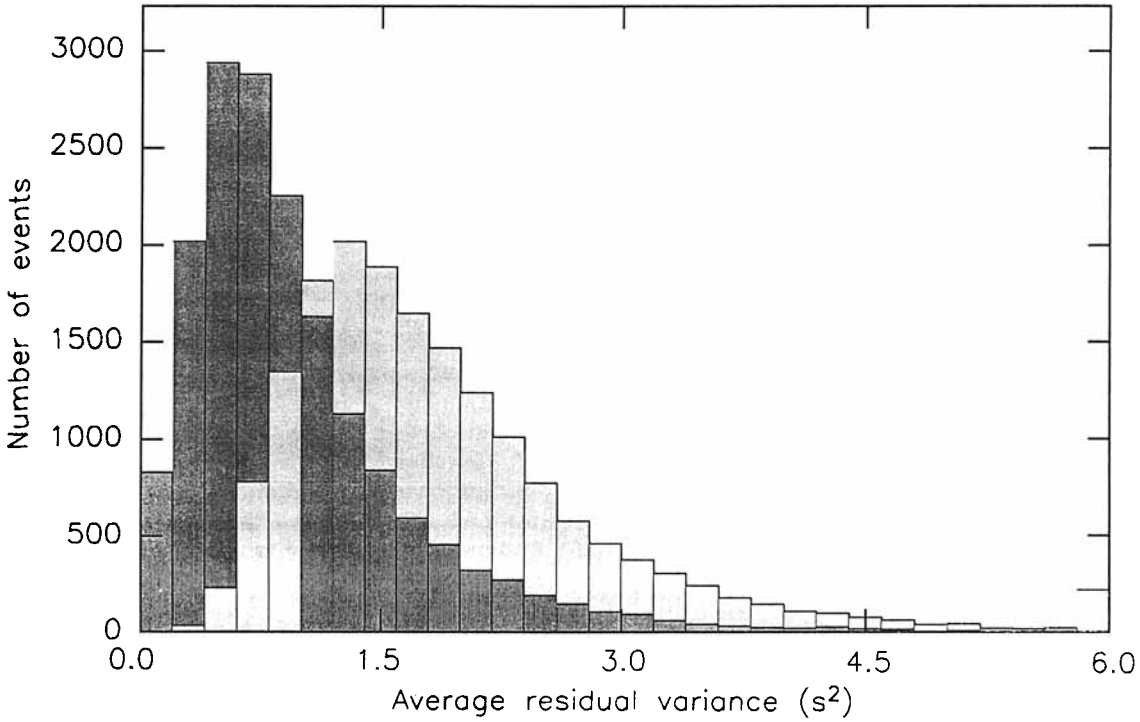

Figure 2. Two, superimposed, histograms of frequency distribution of earthquakes according to residual variance. Lighter bars refer to ISC location, dark grey bars illustrate the situation after relocation with empirical source-station corrections. Residual variance is computed averaging, for each event, the variance of all traveltime residuals after relocation.

in an inversion all the data available, weighting each observation with an estimate of its standard deviation, and possibly using some scheme to account for large residuals, like the uniform reduction (Jeffreys 1932) or some other *ad hoc* procedure. Estimates of standard deviation vary considerably from one phase to another, and should be included to prevent unrealistic features. This inversion procedure, however, has two main drawbacks. First, it is obviously computationally very expensive, especially when dealing with as numerous datasets as the ones involved in this study (Table 1). To derive differential kernels for each earthquake-station path will result in excessive computation time, with no real benefit in a study aimed at the retrieval of average structure.

Further, the direct inversion of the raw dataset may be dangerous when data reliability is uncertain. For instance, two different traveltime branches may cross and the arrivals are misidentified, or when—for some other reason—the density distribution of residuals deviate considerably from theoretical models. In such cases, it is advisable to visually inspect the dataset to make sure that these effects are, as much as possible, taken into account.

Table 1. Number of arrivals selected from ISC Bulletins for the phases used in the construction of time–distance curves. The phase identified as *PKP*1 corresponds to the *PKP* first arrival, and includes both the *DF* (*PKIKP*) and the *BC* branches. *BC* is more energetic and is usually read instead of *DF* in the distance range between 145° and 153°. The phase identified as *PKP*2 corresponds to the *AB* branch.

PHASE	SELECTED ARRIVALS
P	1,554,972
PcP	33,649
PKP1	341,978
PKP2	15,158
S	123,608

The first panel in Fig. 3 shows the distribution of residuals—defined as observed minus computed time in a reference model—for all *P*-wave arrivals selected for epicentral distance between 46.5° and 47.5°. It has been known for a long time that the distribution deviates from the Gaussian, because of longer tails and of the asymmetry due to a late bias in phase picking. The uniform reduction method, first proposed by Jeffreys (1932) for derivation of discrete time–distance curves, takes account of the non-Gaussian shape of the model probability density function by means of a statistical weight. It is based on modelling the observed distribution with the superposition of a Gaussian and one or more other distributions to account for longer tails and asymmetry, and its estimates have been shown to be unbiased and normally distributed (Jeffreys 1932). Uniform reduction was later generalized to deal with multivariate analyses, such as earthquake location (Bolt 1960), and a theory for estimating confidence intervals has been developed (Buland 1986).

The first panel of Fig. 3 shows a very typical shape for a population of teleseismic *P* residuals at a fixed distance. In standard least-square minimizations—correct only under the hypothesis of a normal error distribution—an empirical method commonly used to limit the effect of outliers consists in the truncation of residuals too large, which would

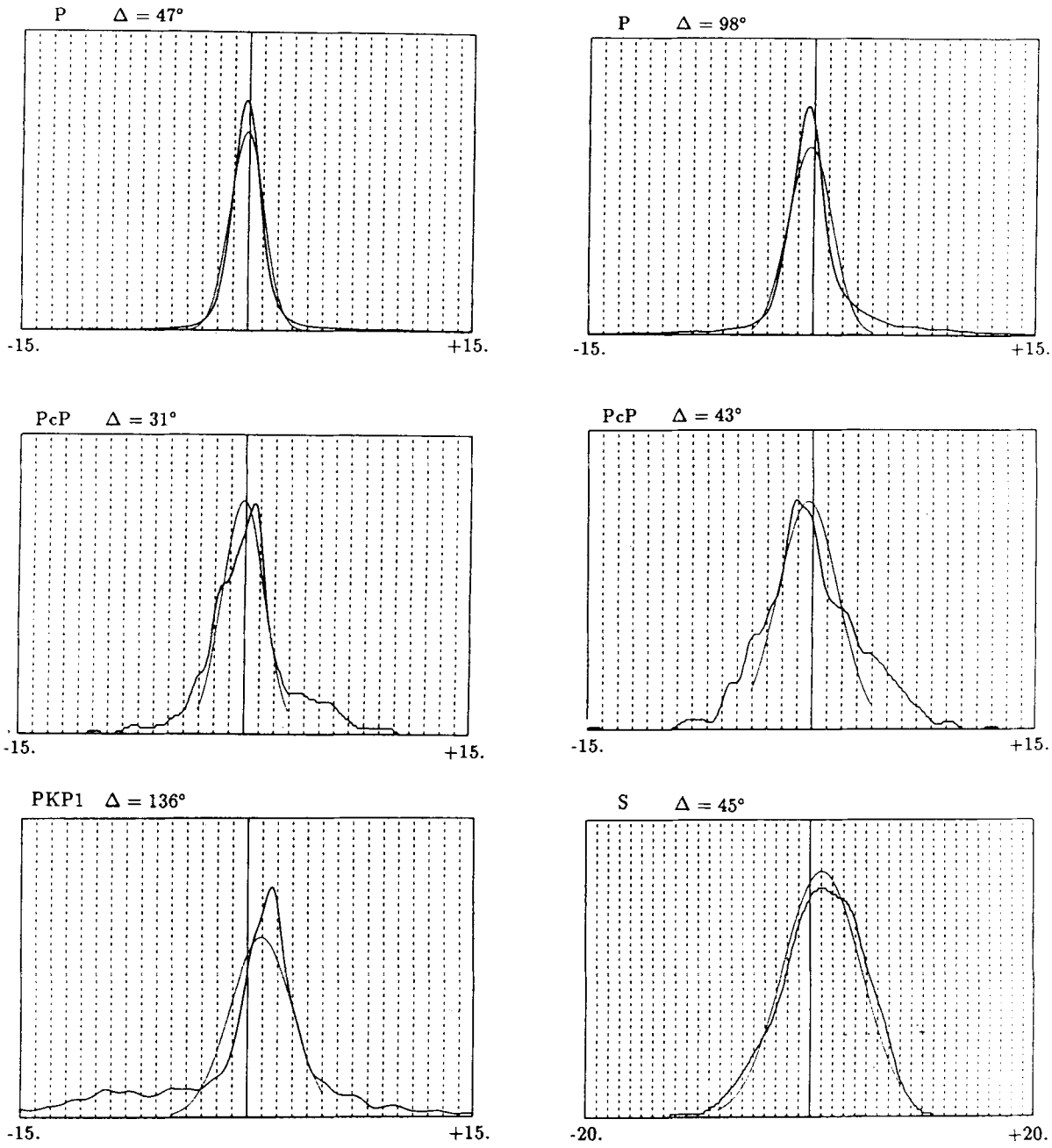

Figure 3. Examples of frequency distributions observed for teleseismic residuals of different phases at fixed distance. Each plot refers to all arrivals in a 1° interval centred on the value indicated. Vertical dashed lines are 1 s apart. The thin curve is the best fitting Gaussian, calculated in the interval—symmetric with respect to 0—where it is plotted (±4*s* for *P*, ±8*s* for *S*). Truncation yields a biased mean when the distribution is not centred or when side bumps are present.

otherwise be overweighted, under the assumption that they result from erroneous readings. The thin curve in Fig. 3 is the best-fitting Gaussian in an interval between −4 and +4 s from the expected arrival time. This is the distribution which a truncated least-square algorithm would fit. The obvious remark is that the two distributions differ, and the Gaussian has a mean slightly shifted with respect to the most populated bin. This effect is more evident in worse-behaved cases, such as the distribution centred on 98° distance also shown in Fig. 3 (top-right panel). The mean residual is later than the observed maximum (most populated value), the truncation interval being centred on the expected (theoretical) value. In an iterative scheme, however, this effect will eventually disappear as the new theoretical value will shift closer to the maximum.

The situation becomes more complicated as we turn to phases more difficult to identify and read, as *PcP*, *PKP* or *S*, even when there is no superposition of two branches (Fig. 3). In these cases it seems impossible to design a specific statistical model to the observed distributions, which vary a good deal in character from one phase to another and from one distance to the next. Studies of the nature of

probability density functions of traveltime residuals have been centred mainly on *P* data, which is the only reasonably well behaved and numerically represented phase (Buland 1984). *PKP* data are contaminated by many effects which complicate their observed distribution. In the *PKP* range even the first arrival phase misidentifications are quite common, with precursors mistakenly picked as a ray-theoretical arrival, and with small-amplitude first arrivals skipped and erroneously associated with a more prominent later phase. On the other hand, the best fitting normal curve in a truncated interval often yields results that may be considerably shifted early or late (see in Fig. 3 *PcP* at 31° and at 43°, where *PcP* and *PP* branches cross), depending on the cause of misidentification.

In a study like this one, which aims to include phases other than *P*, some other scheme must be devised to prevent these potential sources of bias. Our preference is to select interactively for each phase and each 1° bin the most populated value, dealing individually with each histogram and fitting a polynomial to determine the maximum of the histogram. This process is stable and rather objective—certainly much more than picking arrival times from a seismogram. The polynomial representation was chosen because it does not impose any symmetry in the shape. We claim that this is a robust parameter because it is unbiased and does not make any assumption on the statistical properties of the process. An *a posteriori* proof of the validity of this approach is discussed below in the context of Fig. 8. Each 1° distance cell is therefore inspected and evaluated before accepting it as a reliable datum for the inversion. This allows us to deal in optimal way with problems like irregularity in the distribution, or crossing of different branches. The resulting time–distance curves for several phases, (Table 2) represent the data input for the model inversion. It is important to point out that the traveltimes for all the branches have been derived from the same set of relocated earthquakes and therefore have the same baseline. The baseline was adjusted to match that for *P* in *iasp91*, which seems to be a reasonable choice if one assumes that the available test events (Kennett & Engdahl 1991) are representative of the average earth. The summary traveltimes for individual branches are listed in Tables 3 to 8.

Table 2. List of the time–distance curves included in model inversion. Each curve is specified with one value for each 1° bin. For the curves from Hales & Roberts (1970), other than the differential *SKKS–SKS*, a common baseline of 1.4 s is used.

DATASETS USED	
P	this study, 1990
PKIKP	this study, 1990
PKP_{AB}	this study, 1990
PKP_{BC}	this study, 1990
PcP–P	this study, 1990
S	this study, 1990
SKKS–SKS	Hales and Roberts, 1971
S	Hales and Roberts, 1970
SKS	Hales and Roberts, 1970

Table 3. Summary *P* traveltimes at 1° intervals as derived in this study, and computed on the basis of model SP6.

P travel times			
Distance	Observed	Computed	Residual
26	334.50	334.49	0.01
27	343.54	343.54	0.00
28	352.54	352.54	0.00
29	361.44	361.47	-0.03
30	370.29	370.33	-0.04
31	379.13	379.16	-0.03
32	387.94	387.95	-0.01
33	396.68	396.70	-0.02
34	405.42	405.39	0.03
35	414.05	414.04	0.01
36	422.66	422.63	0.03
37	431.19	431.16	0.03
38	439.65	439.63	0.02
39	448.02	448.04	-0.02
40	456.39	456.38	0.01
41	464.69	464.65	0.04
42	472.89	472.85	0.04
43	481.00	480.99	0.01
44	489.08	489.06	0.02
45	497.07	497.05	0.02
46	504.99	504.98	0.01
47	512.82	512.83	-0.01
48	520.61	520.61	0.00
49	528.30	528.32	-0.02
50	535.96	535.95	0.01
51	543.51	543.51	0.00
52	551.00	551.00	0.00
53	558.42	558.42	0.00
54	565.75	565.76	-0.01
55	573.02	573.03	-0.01
56	580.23	580.23	0.00
57	587.36	587.36	0.00
58	594.39	594.41	-0.02
59	601.37	601.39	-0.02
60	608.29	608.29	0.00
61	615.11	615.13	-0.02
62	621.88	621.89	-0.01
63	628.56	628.58	-0.02
64	635.18	635.20	-0.02
65	641.75	641.75	0.00
66	648.21	648.22	-0.01
67	654.60	654.62	-0.02
68	660.93	660.95	-0.02
69	667.18	667.21	-0.03
70	673.38	673.39	-0.01
71	679.50	679.51	-0.01
72	685.55	685.55	0.00
73	691.52	691.52	0.00
74	697.40	697.42	-0.02
75	703.25	703.24	0.01
76	709.01	708.99	0.02
77	714.68	714.67	0.01
78	720.28	720.28	0.00
79	725.83	725.81	0.02
80	731.30	731.27	0.03
81	736.68	736.66	0.02
82	741.99	741.97	0.02
83	747.22	747.21	0.01
84	752.40	752.37	0.03
85	757.47	757.46	0.01
86	762.49	762.47	0.02
87	767.41	767.41	0.00
88	772.26	772.27	-0.01
89	777.03	777.05	-0.02
90	781.77	781.75	0.02
91	786.44	786.40	0.04

Table 3. (continued)

P travel times			
Distance	Observed	Computed	Residual
92	791.09	791.05	0.04
93	795.70	795.69	0.01
94	800.30	800.32	-0.02
95	804.92	804.94	-0.02
96	809.51	809.54	-0.03
97	814.08	814.13	-0.05
98	818.65	818.70	-0.05

The inversion is based on an iterative least-squares optimization. We start with an initial model, m_0, to locate earthquakes and to compute station-source region corrections, such as those of Fig. 1. From residual histograms we produce summary time–distance curves, which we assume to be free from anomalies caused by lateral heterogeneities—neglecting possible small-scale, residual effects. We proceed to invert these data for a new model, m_1, which is then used for subsequent earthquake relocation and derivation of the new summary traveltime curves. These, in turn, are used to derive a new model, m_2. At this stage, we determine that the process has converged and terminate the iterations.

Table 4. Summary *PcP–P* traveltimes at 1° intervals as derived in this study, and computed on the basis of model SP6.

PcP-P differential travel times			
Distance	Observed	Computed	Residual
25	216.34	215.26	1.08
26	209.05	208.42	0.63
27	202.18	201.71	0.47
28	194.59	195.12	-0.53
29	189.47	188.67	0.80
30	182.73	182.36	0.37
31	176.07	176.16	-0.09
32	170.12	170.06	0.06
33	163.80	164.07	-0.27
34	158.15	158.19	-0.04
35	152.09	152.42	-0.33
36	146.85	146.77	0.08
37	141.36	141.25	0.11
38	135.66	135.84	-0.18
39	130.54	130.55	-0.01
40	125.23	125.39	-0.16
41	120.29	120.34	-0.05
42	115.15	115.42	-0.27
43	110.35	110.61	-0.26
44	106.05	105.93	0.12
45	101.70	101.36	0.34
46	97.17	96.91	0.26
47	92.70	92.58	0.12
48	88.34	88.37	-0.03
49	84.39	84.27	0.12
50	80.38	80.28	0.10
51	76.61	76.41	0.20
52	72.69	72.65	0.04
53	69.04	69.00	0.04
54	65.42	65.46	-0.04
55	62.42	62.02	0.40
56	58.89	58.70	0.19
57	55.61	55.47	0.14
58	52.39	52.36	0.03
59	49.61	49.34	0.27
60	46.40	46.43	-0.03
61	43.69	43.61	0.08
62	41.10	40.90	0.20
63	38.65	38.28	0.37
64	36.02	35.76	0.26
65	33.39	33.34	0.05
66	31.36	31.01	0.35
67	28.65	28.77	-0.12

Table 5. Summary PKP_{AB} traveltimes at 1° intervals as derived in this study, and computed on the basis of model SP6.

PKP_{AB} travel times			
Distance	Observed	Computed	Residual
150	1198.61	1198.07	0.54
151	1203.18	1202.21	0.97
152	1207.11	1206.39	0.72
153	1211.37	1210.60	0.77
154	1215.05	1214.84	0.21
155	1219.66	1219.11	0.55
156	1223.96	1223.40	0.56
157	1228.10	1227.71	0.39
158	1232.42	1232.04	0.38
159	1236.57	1236.39	0.18
160	1240.76	1240.75	0.01
161	1245.24	1245.12	0.12
162	1249.70	1249.51	0.19
163	1253.78	1253.90	-0.12
164	1258.19	1258.31	-0.12
165	1262.87	1262.73	0.14
166	1266.78	1267.15	-0.37
167	1271.74	1271.58	0.16
168	1275.81	1276.02	-0.21
169	1280.04	1280.46	-0.42
170	1284.87	1284.91	-0.04
171	1289.90	1289.36	0.54
172	1293.59	1293.81	-0.22
173	1297.84	1298.27	-0.43
174	1302.68	1302.73	-0.05
175	1306.56	1307.19	-0.63

Deriving a model from a set of observed summary traveltime curves is generally an underdetermined problem, and some constraints must be introduced. Constraints may be included directly in the inversion scheme—in the form of the expected parameter covariance—or in a less direct way by *a posteriori* inspection to ascertain whether the inversion did alter the model beyond expected limits. This is the approach that we follow, performing standard damped least-squares inversions and selecting the value of the damping parameter after successive trials and evaluation of the results. Each of the models mentioned above is in fact the result of a number of partial inversions. Each partial inversion (six in the case of SP6) uses a subset of data and perturbs only part of the model. We start with the mantle

Table 6. Summary PKP_{BC} traveltimes at 1° intervals as derived in this study, and computed on the basis of model SP6.

PKP_{BC} travel times			
Distance	Observed	Computed	Residual
145	1178.47	1178.38	0.09
146	1181.46	1181.56	-0.10
147	1184.21	1184.48	-0.27
148	1187.16	1187.24	-0.08
149	1189.85	1189.83	0.02
150	1192.41	1192.29	0.12
151	1194.72	1194.61	0.11
152	1197.10	1196.81	0.29

Table 7. Summary *PKIKP* traveltimes at 1° intervals as derived in this study, and computed on the basis of model SP6.

PKIKP travel times			
Distance	Observed	Computed	Residual
118	1128.70	1128.52	0.18
119	1130.62	1130.46	0.16
120	1132.54	1132.39	0.15
121	1134.38	1134.32	0.06
122	1136.30	1136.25	0.05
123	1138.29	1138.18	0.11
124	1140.20	1140.11	0.09
125	1142.11	1142.04	0.07
126	1144.12	1143.96	0.16
127	1146.13	1145.89	0.24
128	1148.04	1147.81	0.23
129	1149.97	1149.73	0.24
130	1152.01	1151.64	0.37
131	1154.09	1153.55	0.54
132	1155.92	1155.46	0.46
133	1157.96	1157.36	0.60
134	1159.82	1159.26	0.56
135	1161.58	1161.15	0.43
136	1163.47	1163.03	0.44
137	1165.36	1164.91	0.45
138	1167.08	1166.77	0.31
139	1168.98	1168.63	0.35
...	...	...	...
151	1189.52	1189.26	0.26
152	1190.89	1190.77	0.12
153	1192.40	1192.24	0.16
154	1193.70	1193.67	0.03
155	1194.91	1195.05	-0.14
156	1196.23	1196.38	-0.15
157	1197.51	1197.66	-0.15
158	1198.46	1198.89	-0.43
159	1199.79	1200.07	-0.28
160	1200.91	1201.20	-0.29
161	1201.82	1202.27	-0.45
162	1202.94	1203.29	-0.35
163	1204.08	1204.26	-0.18
164	1205.08	1205.17	-0.09
165	1205.78	1206.03	-0.25
166	1206.85	1206.84	0.01
167	1207.81	1207.58	0.23
168	1208.34	1208.28	0.06
169	1209.03	1208.92	0.11
170	1209.90	1209.50	0.40
171	1210.43	1210.03	0.40
172	1210.72	1210.50	0.22
173	1211.29	1210.92	0.37
174	1211.52	1211.28	0.24
175	1211.87	1211.58	0.29
176	1211.97	1211.84	0.13
177	1212.13	1212.03	0.10
178	1212.57	1212.17	0.40
179	1212.08	1212.25	-0.17

Table 8. Summary *S* traveltimes at 1° intervals as derived in this study, and computed on the basis of model SP6.

S travel times			
Distance	Observed	Computed	Residual
26	606.60	606.37	0.23
27	622.82	622.29	0.53
28	637.90	638.05	-0.15
29	653.51	653.77	-0.26
30	669.41	669.47	-0.06
31	685.55	685.12	0.43
32	700.06	700.74	-0.68
33	716.12	716.29	-0.17
34	731.85	731.79	0.06
35	747.05	747.21	-0.16
36	762.49	762.57	-0.08
37	778.22	777.84	0.38
38	793.06	793.03	0.03
39	808.42	808.14	0.28
40	823.19	823.16	0.03
41	837.90	838.09	-0.19
42	852.03	852.92	-0.89
43	867.72	867.66	0.06
44	882.59	882.30	0.29
45	896.27	896.84	-0.57
46	911.79	911.28	0.51
47	925.44	925.61	-0.17
48	939.85	939.84	0.01
49	954.03	953.97	0.06
50	968.73	967.98	0.75
51	981.94	981.90	0.04
52	995.32	995.70	-0.38
53	1009.07	1009.39	-0.32
54	1023.15	1022.98	0.17
55	1036.34	1036.45	-0.11
56	1049.84	1049.82	0.02
57	1063.23	1063.07	0.16
58	1076.11	1076.22	-0.11
59	1089.34	1089.25	0.09
60	1102.21	1102.17	0.04
61	1115.07	1114.98	0.09
62	1128.01	1127.67	0.34
63	1140.31	1140.26	0.05
64	1152.29	1152.73	-0.44
65	1164.98	1165.08	-0.10
66	1177.28	1177.33	-0.05
67	1189.18	1189.46	-0.28
68	1201.75	1201.47	0.28
69	1213.34	1213.37	-0.03
70	1225.12	1225.16	-0.04
71	1237.23	1236.83	0.40
72	1248.49	1248.39	0.10
73	1259.96	1259.83	0.13
74	1271.10	1271.16	-0.06
75	1282.91	1282.36	0.55
76	1293.26	1293.46	-0.20
77	1304.27	1304.43	-0.16
78	1314.87	1315.29	-0.42
79	1326.48	1326.02	0.46
80	1336.08	1336.64	-0.56

with *P* and *S*, and then perturb the core structure using core phases. This approach allows us to trace contributions coming from the different subsets, and to control them.

THE MODEL

Our starting model of the crust and upper mantle is *iasp91* of Kennett & Engdahl (1991). We choose to use only teleseismic traveltimes, and these are insufficient to determine upper mantle velocity. Therefore, the structure of the upper mantle is not the essential objective of this work, and we limit the changes there to the necessary minimum. The starting lower mantle and core structure are derived from a previous model (MD89PSA, Morelli & Dziewonski 1989) which, in turn, was obtained by perturbing the isotropic PREM to fit the ISC summary traveltimes. We will refer to this composite starting model as to SP0.

Model *iasp91* provides a fair fit to *P* and *S* arrivals at regional distances (see Fig. 2 of Kennett & Engdahl 1991). However, the fit to the summary time–distance curves determined in this study is not satisfactory (Fig. 4). In particular, note the variations of *P* times with distance. For distances larger than 80° the *iasp91* times are too fast, with the difference reaching 0.8 s at 100°. Most of the difference, we believe, is due to the significantly higher *P*-wave velocities below 2000 km depth under the Asian continent (Dziewonski 1984; Morelli & Dziewonski 1991, MD91 hereafter). The *iasp91* traveltimes are biased in this epicentral range by the high level of seismicity in the western Pacific recorded by the very dense network of European stations. For teleseismic *S*, there is on average 1 s of difference, *iasp91* being this time too slow.

Core traveltimes, also, do not appear to match our observations. There is no important baseline correction for *P*, but all the *PKP* (*AB*, *BC*, *DF*) are observed on average almost 1 s late with respect to model predictions. Differential traveltimes of *PcP–P* and *SKKS–SKS* are not well reproduced. Differential traveltimes do not suffer from baseline biases and reveal some inadequacy of the model.

During the process which led us to model SP6, the upper mantle was also allowed to vary to match traveltimes in the distance range between 25° and 40°, which arrive earlier than predicted by *iasp91* and which would not be fit otherwise. The changes in upper mantle structure for both v_P and v_S are, however, very small and are limited to the layer between depths of 410 and 660 km (Fig. 5). Model SP6 is described in Tables 9 and 10.

The lower mantle required only smaller changes from starting model SP0. The two models, *iasp91* and SP6, shown in Fig. 6 along with PREM as a reference, produce very similar traveltime curves up to 80° and have no appreciable baseline shift (Fig. 7). They disagree beyond that distance, with SP6 predictions being slower and closely following the trend shown by our summary traveltimes. Apart from a baseline shift, which is well absorbed by the correspondent shift in origin time, these traveltimes are in agreement, and perhaps slightly faster, than those of Dziewonski (1984)

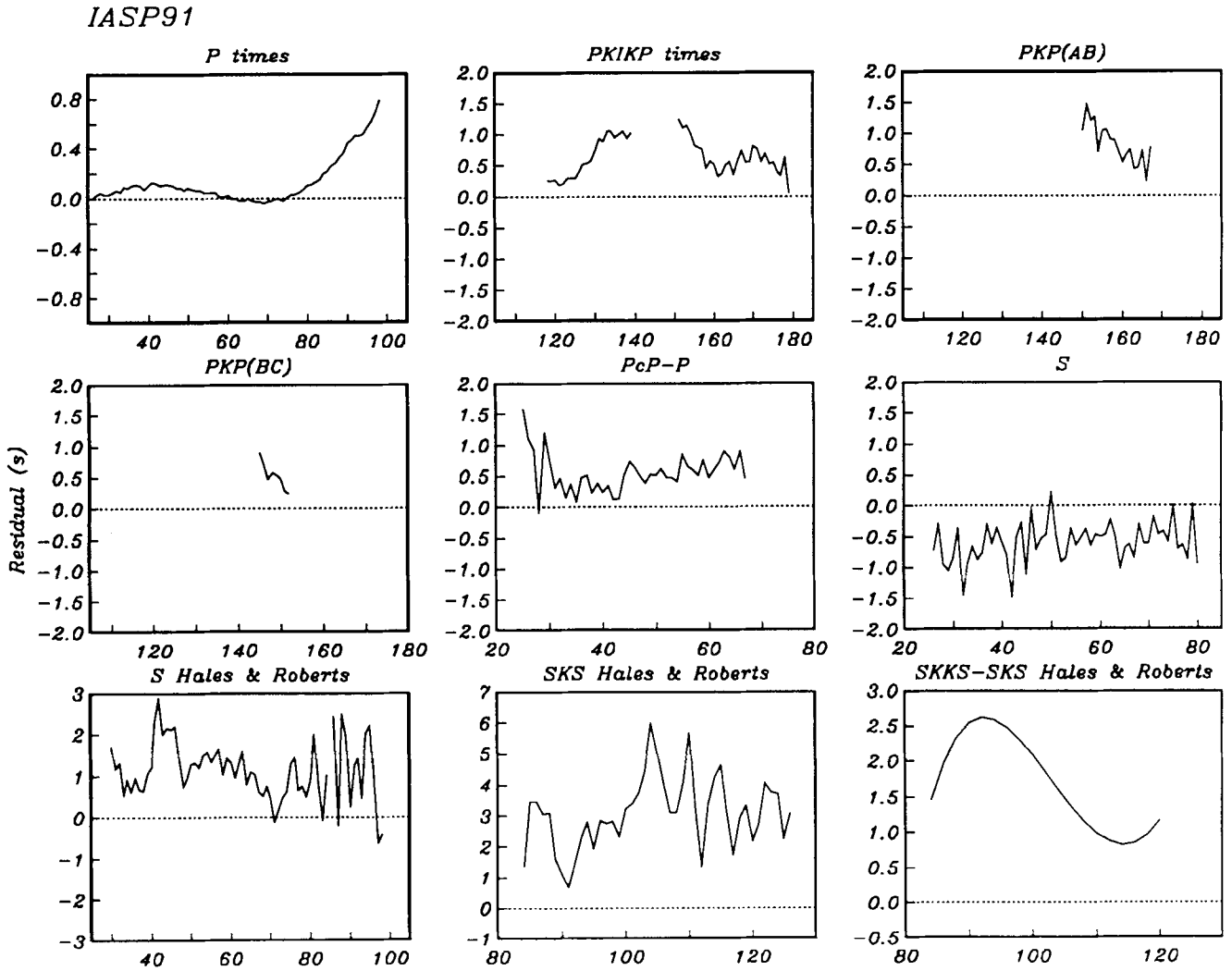

Figure 4. Misfit of the traveltimes for the different phases considered as resulting from the comparison with model *iasp91*. Each residual time is computed as the difference between observed and predicted traveltimes. Residual times are plotted as a function of epicentral distance, expressed in degrees.

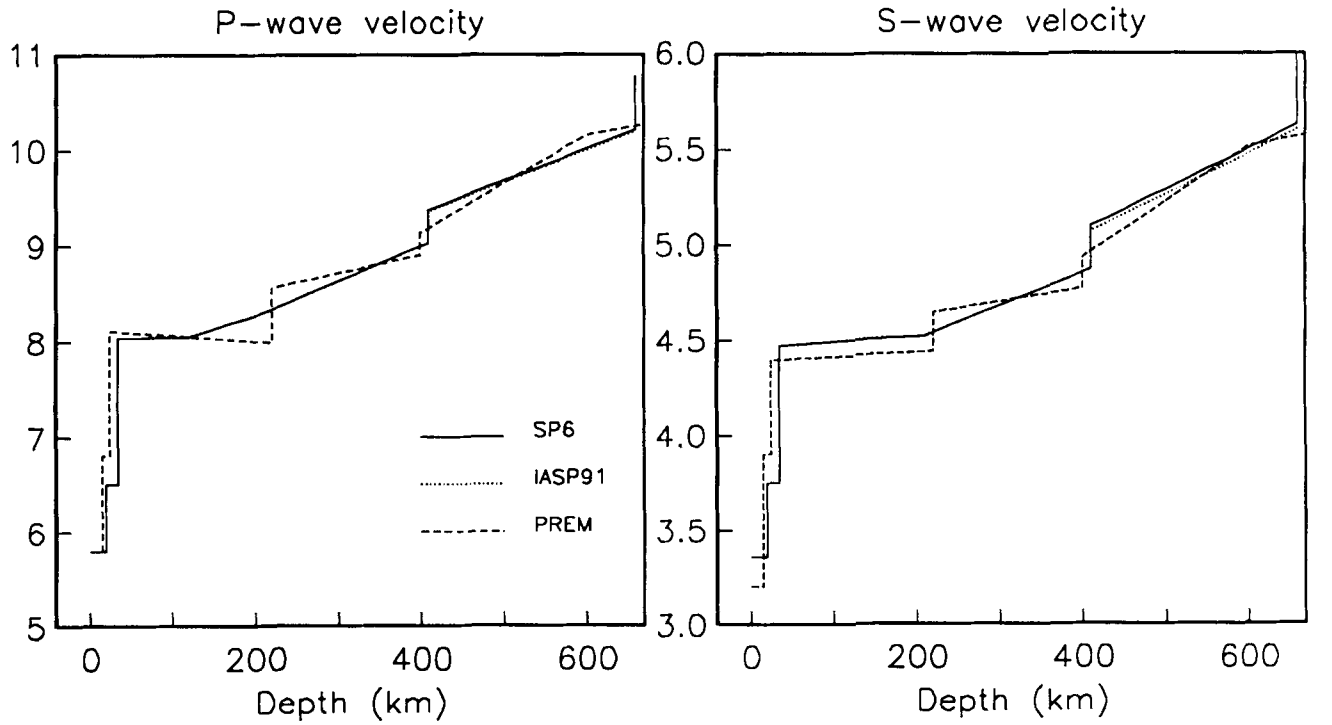

Figure 5. Comparison of models SP6 (continuous line), *iasp91* (dotted line), and isotropic PREM (dashed line) in the upper mantle. The difference of SP6 with respect to *iasp91* is limited to slightly higher velocities between 410 and 660 km. P and S velocity is expressed in km s^{-1}.

Table 9. Coefficients for model SP6. In each of 11 spherical shells v_P and v_S are parametrized by means of a polynomial representation up to degree 3 in normalized radius x. The range for x is from 0 to 1. Depth and radius limits for each shell are listed in the first two columns.

Depth (km)	Radius (km)	v_P (km/s)	v_S (km/s)
0- 20	6351-6371	5.80000	3.36000
20- 35	6336-6351	6.50000	3.75000
35- 120	6251-6336	8.78541 $-0.74953x$	6.70623 $-2.24858x$
120- 210	6161-6251	25.40956 $-17.69281x$	5.75198 $-1.27602x$
210- 410	5961-6161	30.78588 $-23.25239x$	15.24313 $-11.08653x$
410- 660	5711-5961	29.39809 $-21.40010x$	17.72032 $-13.49239x$
660- 771	5600-5711	26.01542 $-17.00747x$	17.57267 $-12.92378x$
771-2741	3630-5600	23.61837 $-35.52920x$ $45.20724x^2$ $-23.92870x^3$	11.87772 $-17.43557x$ $23.32985x^2$ $-12.31633x^3$
2741-2891	3480-3630	12.84645 $1.36611x$	5.65120 $2.78686x$
2891-5156	1215-3480	11.31616 $-7.09314x$ $15.75426x^2$ $-25.70488x^3$	0
5156-6371	0-1215	11.29719 $-8.88699x^2$	3.66780 $-4.44749x^2$

which correspond to $\ell = 0$ term in the spherical harmonic expansion of the lower mantle in model L02.56 (Dziewonski 1984). The traveltimes of Dziewonski & Anderson (1983) were obtained without consideration of lateral heterogeneity, but care was taken not to overemphasize the seismicity in subduction zones. These traveltimes are about half way between those for SP6 and *iasp91*.

The difference between our estimate of the P traveltimes at distances beyond 80° and those of *iasp91* reflects, as already mentioned above, a bias induced by lateral variations in earth structure and uneven geographical data coverage. Rays travelling distances from 90° to 100° reach—and are mostly sensitive to—the lowermost 100–200 km of the mantle, which in the southern hemisphere is on average slower than in the northern (MD91). The relative deficiency of paths sampling the southern hemisphere leads to too fast 'average' summary traveltimes. The procedure that we have followed to derive the current traveltimes accounts for lateral heterogeneity in an empirical way, and our curve represents a more balanced geographical average. We believe that this is an important point in the modelling philosophy outlined in the Introduction.

Incidentally, it is interesting to note that the procedure we use to derive a summary traveltime curve results in very smooth estimates. Fig. 8 shows the residuals, computed with respect to SP6, of our summary traveltimes compared with the degree-by-degree average times reported by Dziewonski (1984). The value of the summary traveltimes has been found in both cases for each degree independently, without any smoothing between neighbouring 1° bins. However, in the present report we have used empirical source

Table 10. Model SP6 evaluated at discrete values of radius.

radius	depth	v_P	v_S
0.	6371.	11.297	3.668
100.	6271.	11.295	3.667
200.	6171.	11.288	3.663
300.	6071.	11.277	3.658
400.	5971.	11.262	3.650
500.	5871.	11.242	3.640
600.	5771.	11.218	3.628
700.	5671.	11.190	3.614
800.	5571.	11.157	3.598
900.	5471.	11.120	3.579
1000.	5371.	11.078	3.558
1100.	5271.	11.032	3.535
1200.	5171.	10.982	3.510
1215.	5156.	10.974	3.506
1215.	5156.	10.358	0.000
1300.	5071.	10.306	0.000
1400.	4971.	10.245	0.000
1500.	4871.	10.184	0.000
1600.	4771.	10.121	0.000
1700.	4671.	10.057	0.000
1800.	4571.	9.990	0.000
1900.	4471.	9.920	0.000
2000.	4371.	9.847	0.000
2100.	4271.	9.769	0.000
2200.	4171.	9.687	0.000
2300.	4071.	9.599	0.000
2400.	3971.	9.506	0.000
2500.	3871.	9.405	0.000
2600.	3771.	9.298	0.000
2700.	3671.	9.183	0.000
2800.	3571.	9.060	0.000
2900.	3471.	8.927	0.000
3000.	3371.	8.785	0.000
3100.	3271.	8.633	0.000
3200.	3171.	8.471	0.000
3300.	3071.	8.297	0.000
3400.	2971.	8.111	0.000
3480.	2891.	7.953	0.000
3480.	2891.	13.593	7.173
3500.	2871.	13.597	7.182
3600.	2771.	13.618	7.226
3630.	2741.	13.625	7.239
3630.	2741.	13.625	7.239
3700.	2671.	13.545	7.208
3800.	2571.	13.432	7.165
3900.	2471.	13.321	7.122
4000.	2371.	13.210	7.079
4100.	2271.	13.099	7.037
4200.	2171.	12.987	6.994
4300.	2071.	12.875	6.951
4400.	1971.	12.761	6.907
4500.	1871.	12.645	6.862
4600.	1771.	12.526	6.815
4700.	1671.	12.404	6.767
4800.	1571.	12.278	6.717
4900.	1471.	12.148	6.665
5000.	1371.	12.012	6.610
5100.	1271.	11.872	6.553
5200.	1171.	11.725	6.492
5300.	1071.	11.571	6.428
5400.	971.	11.411	6.360
5500.	871.	11.243	6.289
5600.	771.	11.066	6.213
5600.	771.	11.066	6.213
5700.	671.	10.799	6.010
5711.	660.	10.770	5.988
5711.	660.	10.215	5.626
5800.	571.	9.916	5.437
5900.	471.	9.580	5.225
5961.	410.	9.375	5.096
5961.	410.	9.030	4.870
6000.	371.	8.888	4.802
6100.	271.	8.523	4.628
6161.	210.	8.300	4.522
6161.	210.	8.300	4.518
6200.	171.	8.192	4.510
6251.	120.	8.050	4.500
6300.	71.	8.044	4.483
6336.	35.	8.040	4.470
6336.	35.	6.500	3.750
6351.	20.	6.500	3.750
6351.	20.	5.800	3.360
6371.	0.	5.800	3.360

region—station corrections, and carefully picked the traveltime for each distance. This seems to remove much of the scatter. After the inversion, our traveltimes have a residual variance of 0.00043 s^2 (standard deviation 0.02 s) which can be compared with the value of 0.031 s^2 (standard deviation 0.17 s) for the set of Dziewonski (1984). The agreement of the general trend of the two sets, out to 100°, is an important check, also in view of the differences between the two studies in computing the degree-by-degree averages and in accounting for lateral heterogeneity. The agreement confirms our statement that the slight increase in average traveltimes beyond 90° results from consideration of lower mantle heterogeneity.

The *S*-velocity in the lower mantle, in comparison with PREM, follows the trend of the *P*-velocity (see Fig. 6). Predicted traveltimes (Fig. 9) are very similar to those produced by *iasp91,* with only a constant time shift of about 0.5 s. This is a rather small disagreement for *S*.

The core radius is 3480 km, the same value as in PREM. We did not find the need to change it, considering the good fit to the *PcP–P* data. The differential *PcP–P* data were obtained subtracting the times of the two phases from each actual event-station pair, and are therefore not influenced by the uncertainties in the origin time and, within reason, the focal depth. The predictions of *iasp91,* which are systematically faster by about 0.5 s than our observations, are consistent with our inference that the lowermost mantle, to which *PcP–P* is sensitive, is too fast in that model.

Outer core structure has changed slightly to improve the fit to PKP_{AB}, PKP_{BC} and *SKKS–SKS*. PKP_{BC} data are well fitted (Fig. 10) but a negative linear trend in PKP_{AB} residuals appears quite significant. It has been impossible to reduce it with the current parametrization while maintaining a good fit to the other core data. A better fit to *AB* alone could be obtained increasing wave speed at the top of the outer core and decreasing it considerably at the bottom. This, however, would degrade the fit to all the other phases. The misfit for the *AB* branch is most likely a result of some structural complication, either radial or lateral, possibly close to the core–mantle boundary, to which PKP_{AB} is very sensitive. *SKKS–SKS* from Hales & Roberts (1971) are fit within the variance shown by the data. Also *S* and *SKS* from Hales and Roberts are shown in Fig. 10, but were never used in the inversion. The curves shown have a common arbitrary baseline of 1.4 s subtracted, and match the model rather well. There is, on average, a 2.5–3 s difference between the predictions of SP6 and *iasp91* for *SKS* between 84° and 126°.

PKIKP times in the starting model SP0 were about 0.5 s too early when compared to the summary data. An attempt to reduce this shift by modifying *P* velocity in the outer core

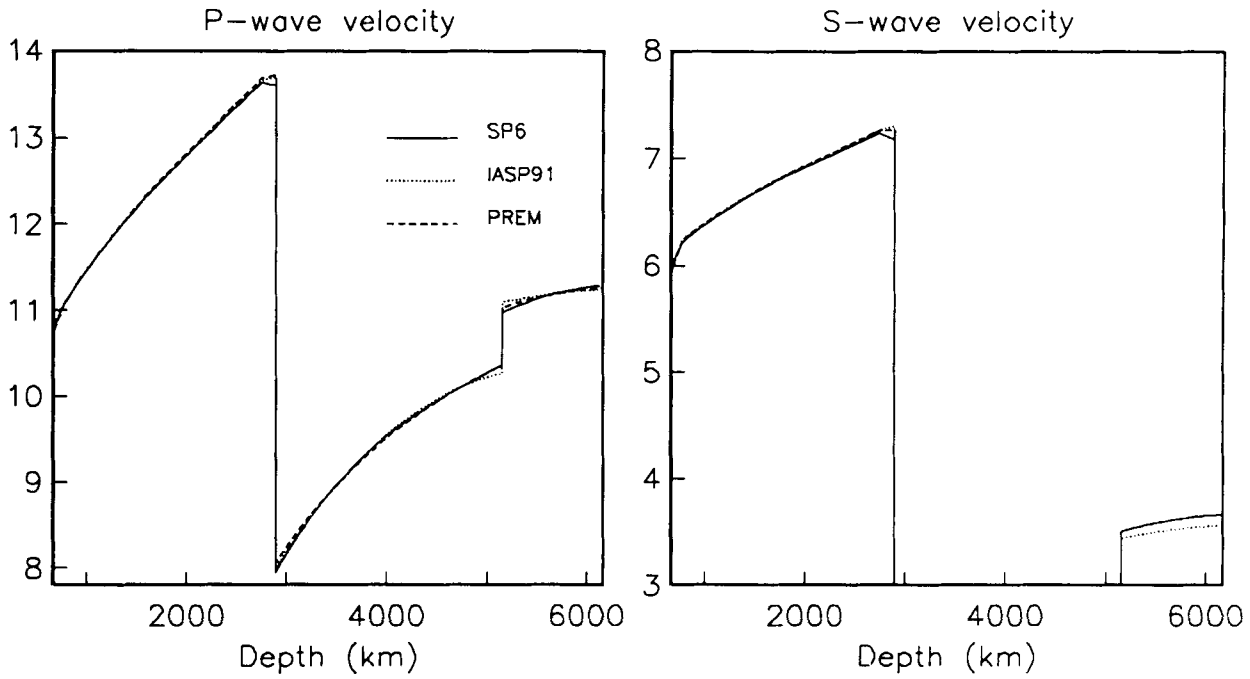

Figure 6. Comparison of models SP6 (continuous line), *iasp91* (dotted line), and isotropic PREM (dashed line) in the lower mantle.

would degrade considerably the fit to other *PKP* and to *SKKS–SKS* data. To make predicted *PKIKP* times longer it is not sufficient to change the velocity structure of the inner core. Short distance rays—distance less than, say, 130°—travel inside the inner core only a very short interval and are only slightly affected by a change in v_P there. As a result, decreasing wave velocity in the inner core reduces only residuals at distance greater than 145°. To make predicted *PKIKP* times longer at short distances we have to decrease the radius of the inner core—a change which affects large distance arrivals much less. As a consequence, the inner core radius was changed to 1215 km, a value 6 km smaller than in PREM and, in addition, v_P in the inner core was also reduced. Inclusion of corrections for inner core anisotropy (Morelli, Dziewonski & Woodhouse 1986; Shearer, Toy & Orcutt 1988) would not alter this situation. The resulting traveltime curves are plotted in Fig. 11 compared to *iasp91* and PREM. The change in *P* velocity at the inner core boundary in SP6 is consistent with the estimates of Cummins & Johnson (1988). For lack of appropriate traveltime data, inner core *S*-velocity profile is assumed to be the same as PREM.

The value of 1215 km for the inner core radius is consistent with the most recent findings from the analysis of differential *PKiKP–PcP* times by Souriau & Souriau (1989). It is interesting that they found a value of 1215.6 km only

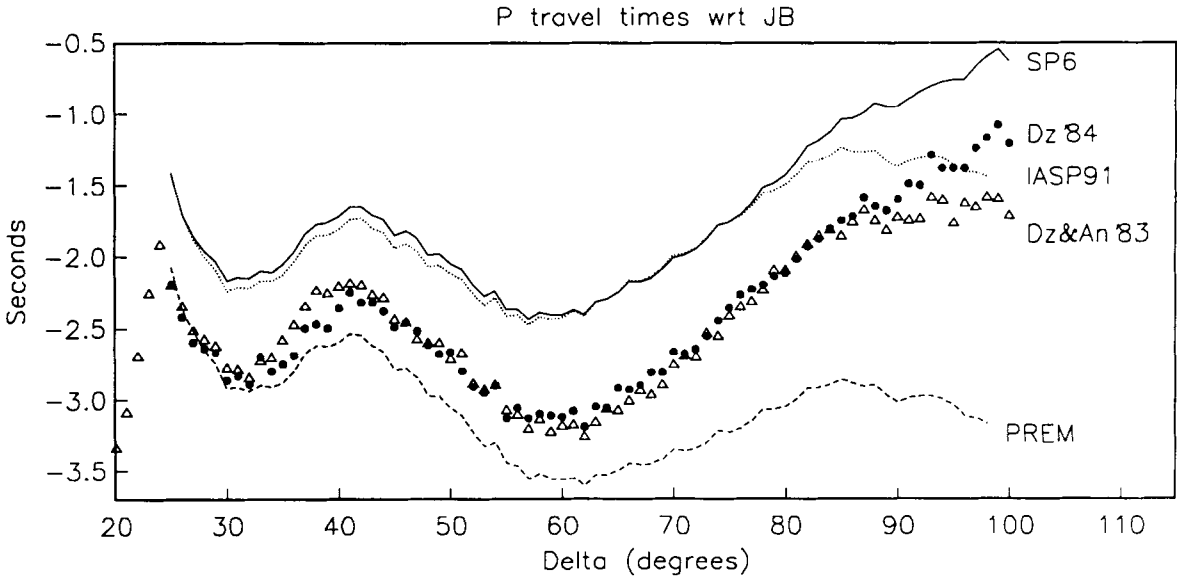

Figure 7. Traveltime curves for *P* waves computed for models SP6 (continuous line), *iasp91* (dotted line), and PREM (dashed line). Also summary traveltimes from Dziewonski & Anderson (1981, open triangles) and Dziewonski (1984, solid circles) are plotted.

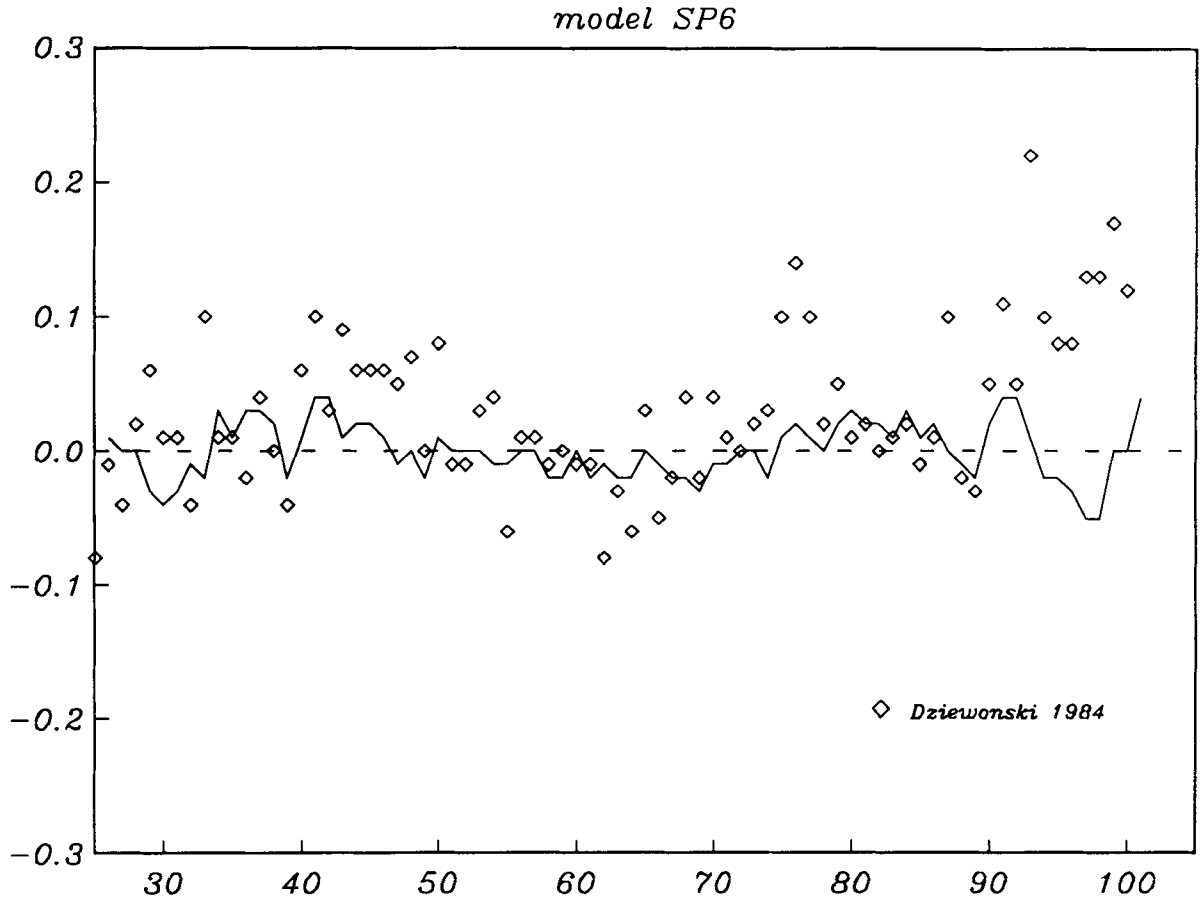

Figure 8. Residual traveltimes, as computed with respect to predictions from SP6, for the set of Table 3 (continuous line) and for the set computed by Dziewonski (1984, diamonds). An arbitrary time shift of 0.7 s has been added to the latter set to facilitate comparison.

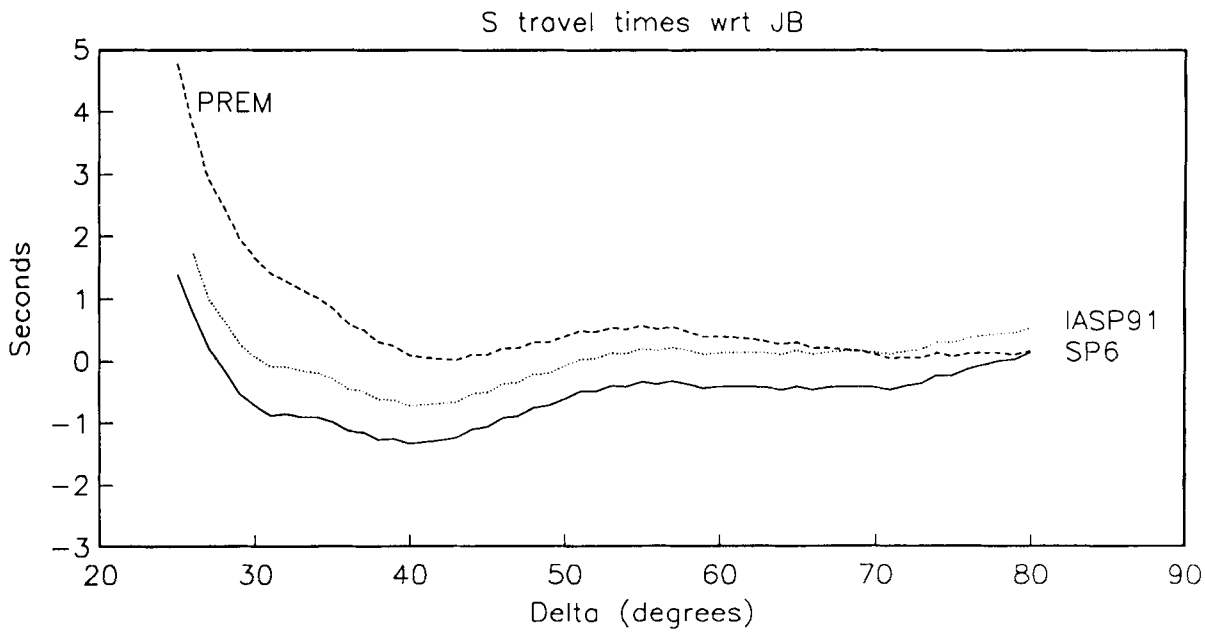

Figure 9. Traveltime curves for *S* waves computed for models SP6 (continuous line), *iasp91* (dotted line), and PREM (dashed line).

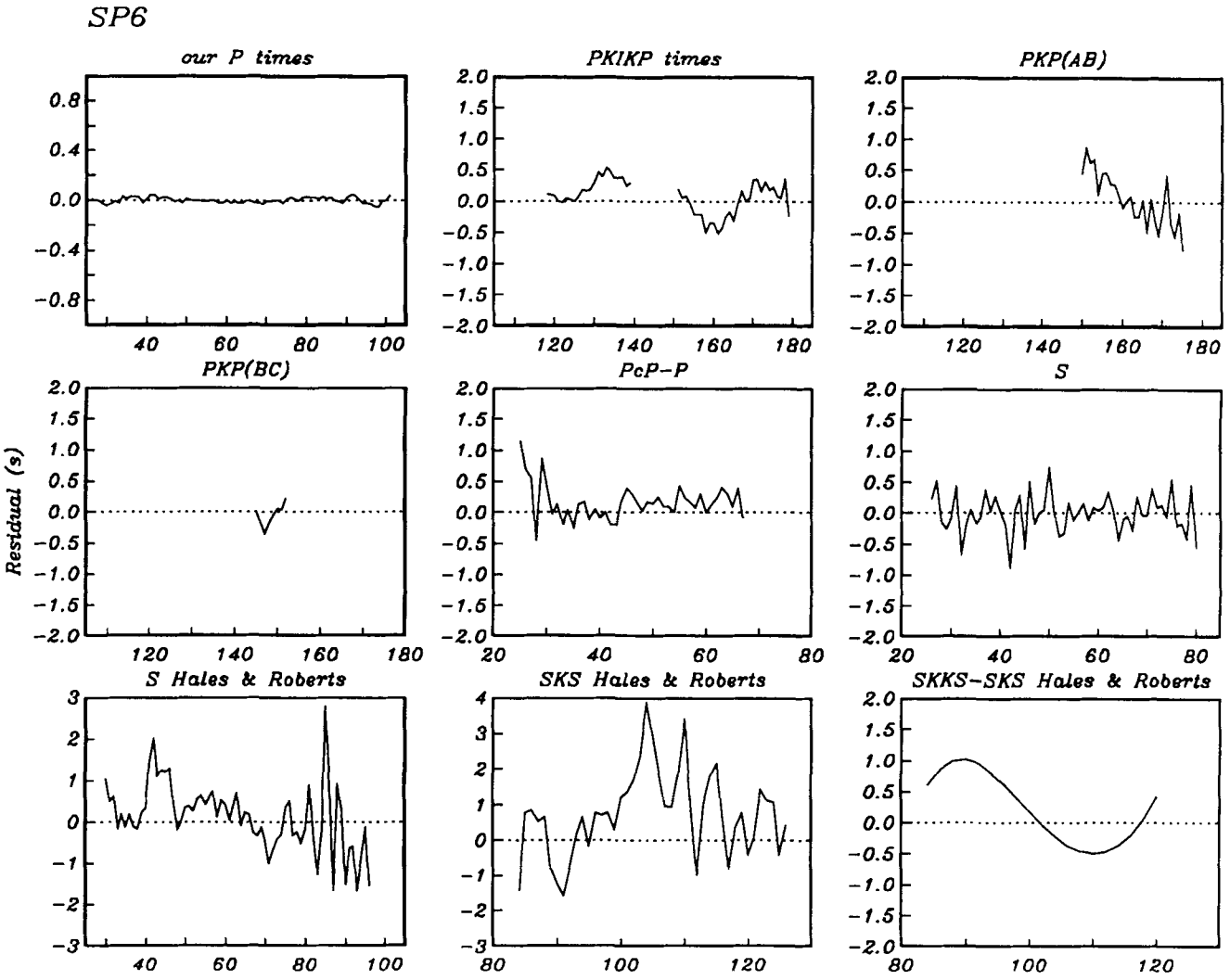

Figure 10. Misfit of the traveltimes for the different phases as resulting from the comparison with model SP6. Same convention as in Fig. 4. A common baseline of 1.4 s has been subtracted from *S* and *SKS* from Hales & Roberts (1970).

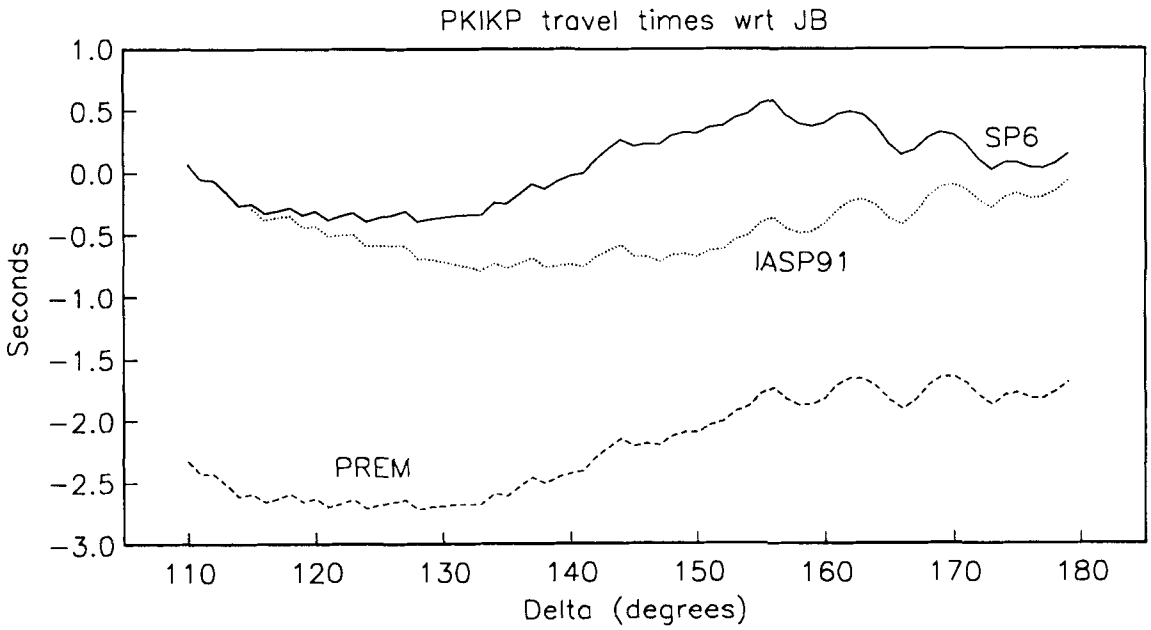

Figure 11. Traveltime curves for *PKIKP* waves computed for models SP6 (continuous line), *iasp91* (dotted line), and PREM (dashed line).

when they apply to the observed data a correction for core–mantle boundary (CMB) undulations using the model of Morelli & Dziewonski (1987), which improves the coherence of their signals. The CMB model of Morelli & Dziewonski also includes a spherical correction of −2.5 km to the PREM value and this was considered by Souriau & Souriau. However, our *PcP–P* times are biased positively when compared to PREM predictions; the difference in *PcP–P* predictions between PREM and SP6 is mainly due to differences in *D″* velocity structure. So, when using PREM mantle velocities, the best fitting CMB radius should be made smaller, as presented in Morelli & Dziewonski (1987) and as used by Souriau & Souriau (1989). The new mantle structure of SP6 agrees with $r_{CMB} = 3480$ km, just like PREM mantle velocities now appear to require a 2.5 km decrease in r_{CMB}. So, we believe that both the inner and outer core radii of SP6 are consistent with Souriau & Souriau (1989) and Morelli & Dziewonski (1987).

Previous determinations of the inner core radius (Engdahl, Flynn & Romney 1970; Engdahl, Flynn & Massè 1974) were based only on reflections from a geographically limited region in the inner core boundary, and therefore are not representative of a global average. The work of Souriau & Souriau is the first attempt to derive both the mean radius and the flattening of the inner core together. It is interesting to note that the same value of r_{CMB} is obtained here from an analysis of *PKIKP* times reported by the ISC, a dataset which has a much better geographical coverage than *PKiKP*.

DISCUSSION AND CONCLUSIONS

Model SP6 differs only slightly from the upper mantle in *iasp91* and from PREM in the lower mantle and core. Here, velocity profiles have, in general, more curvature. The fit to the summary traveltime data is good, with only minor features still left unmodelled. The *P*-wave traveltimes are well matched by perturbing PREM lower mantle and, only slightly, *iasp91* upper mantle. PKP_{AB} residuals still retain a negative trend with increasing distance, which could be eliminated by an unrealistic v_P increase in *D″*. This may be the effect of strong lateral variations in structure of *D″*, to which PKP_{AB} is very sensitive. The outer core velocity also fits *SKKS–SKS* data from Hales and Roberts (1971).

In the *D″* region the new model SP6 is characterized by negative gradients for both v_P and v_S, necessary to reproduce traveltimes at large distances. Traveltimes beyond 80° appear to average to slower values when lateral variations are allowed in lower mantle structure. This is verified by the comparison of the present study with the times published by Dziewonski (1984). Reduced or negative gradients are consistent with the view of *D″* as a thermal boundary-layer with an increased temperature gradient (Stacey & Loper 1983) and have already been proposed in other seismic models. Evidence for other structural complications at the base of the mantle, like a discontinuity with a positive jump in v_S and v_P about 250 km above the CMB, is still subject of debate (Lay 1986; Young & Lay 1990; Schlittenhardt, Schweitzer & Müller 1985; Schlittenhardt 1986). It is most likely to be a regional rather than a global feature (Davis & Weber 1990), a hypothesis confirmed by the considerable variation seen in velocities at the base of the *D″* layer (Dziewonski 1984, MD91; Wysession & Okal 1989). The present study is not able to resolve the fine structure of the base of the mantle—for instance, the thickness of *D″* has been constrained to be 150 km as in PREM. However, it now seems sensible to assume that any study of that region conducted in greater detail will have to consider lateral variations, in the form of a global model or of a regionalization, that are outside the goals of the present study. Within the resolution allowed by traveltimes alone, and fixing *D″* thickness, we found it impossible to reproduce our empirical time–distance curves without a negative velocity gradient at the base of the mantle. We emphasize that this is to be meant solely as a global average, which can—and is likely to—vary considerably in different regions.

The summary time–distance curves used to compute model SP6 were found employing corrections for lateral heterogeneity. If one were to use SP6 for earthquake location—and we emphasize that this alone was not the main objective of this work—the procedure should optimally include the empirical source-station corrections found jointly with the model by means of the iterative scheme outlined above. The form of these corrections allow each seismic station to use its own tabulated values for sources located anywhere (see Fig. 1), whereas the weighting scheme proposed eliminates the effect of sharp edges between source regions. However, even though this procedure would increase precision in hypocentre location, as shown in Fig. 2, SP6 has been derived as a completely self-contained earth model. It can be used independently from the heterogeneity corrections equally well as—or better than—*iasp91*. For teleseismic *P* there should be no baseline bias, since it was adjusted to agree with *iasp91*, which was in turn tuned to fit accurately timed nuclear explosions. As empirical traveltimes for the different phases were all computed together, SP6 is internally consistent, and the usual allowance for arbitrary time shifts of each phase (Dziewonski & Anderson 1981) is unnecessary. All seismic phases can, therefore, be consistently used together to locate events.

There is some ambiguity in the definition of what a 'good' model means. The most obvious answer is that it is the best fit to the whole dataset available, for instance in the least-squares sense. Given the uneven sampling of the structure provided by seismicity, however, some local anomalies will be sampled more frequently than others. They will consequently be more weighted, and the model will be biased toward them. As an example, the number of individual source–receiver paths is considerably larger in the northern than in the southern hemisphere. Large-scale *P*-velocity inversions (see MD91) showed that the southern hemisphere is on average slower than the northern, and it would, therefore, be underestimated in the averaging process, because it will be weighted by a smaller number of paths. The average model will be biased towards northern hemisphere *P* velocity: the best least-squares model will not be the closest to the *physical* average.

On the other hand, it is to some extent possible to account for the non-uniformity of sampling. One solution is to produce summary paths which average individual rays connecting the same pairs of source and receiver regions and to correct for lateral heterogeneity—as was done in MD91.

In this case, the model will represent the average in a more proper sense, because the likelihood to fit a single traveltime observation will not now depend on the number of previous observations for the particular path. Its least-squares fit to the body of all individual observations will, however, be worse than the previous one. We believe that this simple consideration should be taken into account, for instance, when setting up experiments to measure the performance of a model.

The approach that we followed to fit traveltime data—fitting interactively constructed summary time–distance curves—is more reliable than a direct weighted minimization. Its robustness is shown by the resulting limited roughness of the curves, which could be fitted by a parametrically simple model. In case of intersecting branches, it is usually possible to identify the two peaks merging together or splitting away. This allows a more reliable determination of the most frequent value even when the observed distribution has a very deformed shape.

A new reference model should also satisfy users other than those interested in earthquake location using reported arrival times. It is important that additional observations be considered to test models and they should be included in the inversion. Long and ultra-long period waveform studies provide valuable independent information on the earth structure and earthquake mechanism. The centroid–moment tensor (CMT) project carried out at Harvard for the last decade (Dziewonski *et al.* 1991) may be used as an example. The earthquake-source mechanism and centroid location are determined simultaneously in a non-linear least-squares inversion (Dziewonski, Chou & Woodhouse 1981). The waveforms are corrected for lateral heterogeneity (Woodhouse & Dziewonski 1984), which improves the reliability of the source centroid and the earthquake-moment tensor. Dziewonski & Ekström (1992) have used combined data sets of waveforms and traveltimes to obtain improved earthquake locations in nearly real time. It is clearly desirable that the same model is used in processing each of the two sets. Also, construction of lateral heterogeneity models may require the knowledge of earthquake location and source mechanism (Woodhouse & Dziewonski 1984; Su & Dziewonski 1991). The two inverse processes use the same reference earth model which—since waveform modelling involves summation of normal modes—must contain information not only on the P- and S-velocities but also on density and attenuation.

Comparison of the CMT locations with those obtained using the first arrivals of short-period body waves could be of interest, since it could provide us with information on the spatio–temporal dimensions of the source. Regardless of the potential problems with the lateral heterogeneity, the attempt to do so now is doomed to fail, since different models are used to obtain the hypocentral information from arrival times and to derive the CMT solution. We feel that there is a need to produce a new reference earth model, similar in concept to PREM, which would reflect the progress in our knowledge of traveltimes, normal mode eigenfrequencies and attenuation accumulated in 11 years since the last reference model was constructed. Our much improved understanding of lateral heterogeneity in the earth's interior, and the ways to deal with it, should be taken into consideration.

Equipped with such a reference model, it is desirable to develop a set of empirical station–source region corrections, which could lead to a significant improvement in the precision with which earthquakes are located. A parallel development of a set of 'test events' (Kennett & Engdahl 1991) is also most valuable, because this may be the only way to improve precision of absolute locations. Yet, for such an approach to become practically useful, the distribution of test events must be much more even than that shown in Fig. 4 of Kennett & Engdahl. Even though those authors state that 'The test events provide a reasonable geographic coverage of the globe. . . ,' about 80 per cent of them are contained between 30°N and 60°N, and only five out of 104 events are located in the southern hemisphere. It might be worthwhile to consider an extension of the objectives of the International Seismic Observing Period (Engdahl 1989) to include specific experiments designed to provide good global coverage with the 'test events'.

ACKNOWLEDGMENTS

We thank Enzo Boschi for continuing discussions and encouragement. This research was supported in part by grant EAR90-05013 from the National Science Foundation.

REFERENCES

Adams, R. D., Hughes, A. A. & McGregor, D. M., 1982. Analysis procedures at the International Seismological Centre, *Phys. Earth planet. Interiors.*, **30,** 85–93.

Bolt, B. A., 1960. The revision of earthquake epicentres, focal depths and origin times using a high-speed computer, *Geophs. J. R. astr. Soc.*, **3,** 433–440.

Buland, R., 1984. Residual statistics, *Terra Cognita*, **4,** 268.

Buland, R., 1986. Uniform reduction error analysis, *Bull. seism. Soc. Am.*, **76,** 217–230.

Cummins, P. & Johnson, L. R., 1988. Short-period body wave constraints on properties of the Earth's inner core boundary, *J. geophys. Res.*, **93,** 9058–9074.

Davis, J. P., & Weber, M., 1990. Lower mantle velocity inhomogeneity observed at GRF array, *Geophys. Res. Lett.*, **17,** 187–190.

Dziewonski, A. M., 1984. Mapping the lower mantle: determination of lateral heterogeneity in P velocity up to degree and order 6, *J. geophys. Res.*, **89,** 5929–5952.

Dziewonski, A. M. & Anderson, D. L., 1981. Preliminary Earth reference model, *Phys. Earth planet. Interiors*, **25,** 297–356.

Dziewonski, A. M. & Anderson, D. L., 1983. Travel times and station corrections for P waves at teleseismic distances, *J. geophys. Res.*, **88,** 3295–3314.

Dziewonski, A. M. & Ekström, G., 1992. Joint CMT inversion using waveforms and arrival times, *EOS Trans. Am. Geophys. Un.*, **73,** 193.

Dziewonski, A. M. & Morelli, A., 1989. A basis for global joint hypocenter determination, *EOS Trans. Am. Geophys. Un.*, **70,** 1231.

Dziewonski, A. M., Chou, T.-A. & Woodhouse, J. H., 1981. Determination of earthquake source parameters from waveform data for studies of global and regional seismicity, *J. geophys. Res.*, **86,** 2825–2852.

Dziewonski, A. M, Ekström, G., Woodhouse, J. H. & Zwart, G., 1991. Centroid moment tensor solutions for October–December 1990, *Phys. Earth planet. Interiors*, **68,** 201–214.

Engdahl, E. R., 1989. Coordinating global seismic network observations, *EOS, Trans. Am. Geophys. Un.*, **70,** 1501.

Engdahl, E. R., Flynn, E. A. & Romney, C. F., 1970. Seismic waves reflected from the Earth's inner core, *Nature*, **228,** 852–853.

Engdahl, E. R., Flynn, E. A. & Massè, R. P., 1974. Differential *PKiKP* traveltimes and the radius of the inner core, *Geophys. J. R. astr. Soc.*, **39,** 457–463.

Hales, A. L. & Roberts, J. L., 1970. The travel times of *S* and *SKS*, *Bull. seism. Soc. Am.*, **60,** 461–489.

Hales, A. L. & Roberts, J. L., 1971. The velocities in the outer core, *Bull. seism. Soc. Am.*, **61,** 1051–1060.

Jeffreys, H., 1932. An alternative to the rejection of observations, *Proc. R. Soc. Lond.*, **187,** 78–87.

Jeffreys, H. & Bullen, K. E., 1940. *Seismological Tables*, British Association for the Advancement of Science, London.

Kennett, B. L. N., 1988. Quakes to have better locations, *EOS Trans. Am. Geophys. Soc.*, **69,** 1571.

Kennett, B. L. N. & Engdahl, E. R., 1991. Traveltimes for global earthquake location and phase identification, *Geophys. J. Int.*, **105,** 429–465.

Lay, T., 1986. Evidence of a lower mantle shear velocity discontinuity in *S* and *sS* phases, *Geophys. Res. Lett.*, **13,** 1493–1496.

Morelli, A. & A. M. Dziewonski, 1987. Topography of the core–mantle boundary and lateral homogeneity of the liquid core, *Nature*, **325,** 678–683.

Morelli, A. & Dziewonski, A. M., 1989. Spherically symmetric *P*- and *S*-wave velocity models derived from ISC travel times, Abstracts Volume of the *XXV General Assembly of the International Association of Seismology and Physics of the Earth's Interior*, Instanbul (Turkey), August 21–September 1, 589.

Morelli, A., & Dziewonski, A. M., 1991. Joint determination of lateral heterogeneity and earthquake location, in *Glacial isostasy, sea-level change and mantle rheology*, pp. 515–534, eds R. Sabadini, K. Lambeck & E. Boschi, Kluwer Academic, Dordrecht.

Morelli, A., Dziewonski, A. M. & Woodhouse, J. H., 1986. Anisotropy of the inner core inferred from *PKIKP* travel times, *Geophys. Res. Lett.*, **13,** 1545–1548.

Schlittenhardt, J., 1986. Investigation of the velocity and *Q*-structure of the lowermost mantle using *PcP*/*P* amplitude ratios from arrays at distances of 70°–84°, *J. Geophys.*, **60,** 1–18.

Schlittenhardt, J., Schweitzer, J. & Müller, G., 1985. Evidence against a discontinuity at the top of *D″*, *Geophys. J. R. astr. Soc.*, **81,** 295–306.

Shearer, P. M., Toy, K. M. & Orcutt, J. A., 1988. Axi-symmetric earth models and inner-core anisotropy, *Nature*, **333,** 228–232.

Souriau, A. & Souriau, M., 1989. Ellipticity and density at the inner core boundary from subcritical *PKiKP* and *PcP* data, *Geophys. J. Int.*, **98,** 39–54.

Stacey, F. D. & Loper, D. E., 1983. The thermal boundary layer interpretation of *D″* and its role as a plume source, *Phys. Earth planet. Interiors*, **33,** 45–55.

Su, W.-J. & Dziewonski, A. M., 1991. Predominance of long-wavelength heterogeneity in the mantle, *Nature*, **352,** 121–126.

Woodhouse, J. H. & Dziewonski, A. D., 1984. Mapping the upper mantle: three-dimensional modeling of Earth structure by inversion of seismic waveforms, *J. geophys. Res.*, **89,** 5953–5986.

Wysession, M. E. & Okal, E. A., 1989. Regional analysis of *D″* velocities from the ray parameters of diffracted *P* profiles, *Geophys. Res. Lett.*, **16,** 1417–1420.

Young, C. J. & Lay, T., 1990. Multiple phase analysis of the shear velocity structure in the *D″* region beneath Alaska, *J. geophys. Res.*, **95,** 17 385–17 402.